

Ratchet transport of self-propelled chimeras in an asymmetric periodic structure

Wei-Jing Zhu(朱薇静) and Bao-Quan Ai(艾保全)

Citation: Chin. Phys. B, 2022, 31 (**4**): 040503. DOI: 10.1088/1674-1056/ac3391
Journal homepage: http://cpb.iphy.ac.cn; http://iopscience.iop.org/cpb

What follows is a list of articles you may be interested in

Transport of velocity alignment particles in random obstacles

Wei-jing Zhu(朱薇静), Xiao-qun Huang(黄小群), Bao-quan Ai(艾保全)
Chin. Phys. B, 2018, 27 (**8**): 080504. DOI: 10.1088/1674-1056/27/8/080504

Current transport and mass separation for an asymmetric fluctuation system with correlated noises

Jie Wang(王杰), Li-Juan Ning(宁丽娟)
Chin. Phys. B, 2018, 27 (**1**): 010501. DOI: 10.1088/1674-1056/27/1/010501

An image encryption scheme based on three-dimensional Brownian motion and chaotic system

Xiu-Li Chai(柴秀丽), Zhi-Hua Gan(甘志华), Ke Yuan(袁科), Yang Lu(路杨), Yi-Ran Chen(陈怡然)
Chin. Phys. B, 2017, 26 (**2**): 020504. DOI: 10.1088/1674-1056/26/2/020504

Current and efficiency optimization under oscillating forces in entropic barriers

Ferhat Nutku, Ekrem Aydiner
Chin. Phys. B, 2016, 25 (**9**): 090501. DOI: 10.1088/1674-1056/25/9/090501

Current and efficiency of Brownian particles under oscillating forces in entropic barriers

Ferhat Nutku, Ekrem Aydıner
Chin. Phys. B, 2015, 24 (**4**): 040501. DOI: 10.1088/1674-1056/24/4/040501

Ratchet transport of self-propelled chimeras in an asymmetric periodic structure

Wei-Jing Zhu(朱薇静)[1,†] and Bao-Quan Ai(艾保全)[2,‡]

[1] *School of Photoelectric Engineering, Guangdong Polytechnic Normal University, Guangzhou* 510665, *China*

[2] *Guangdong Provincial Key Laboratory of Quantum Engineering and Quantum Materials, School of Physics and Telecommunication Engineering, South China Normal University, Guangzhou* 510006, *China*

(Received 9 August 2021; revised manuscript received 29 September 2021; accepted manuscript online 27 October 2021)

We studied the rectified transport of underdamped particles subject to phase lag in an asymmetric periodic structure. When the inertia effect is considered, it is possible to observe reversals of the average velocity with small self-propelled force, whereas particles always move in the positive direction with large self-propelled force. The introduction of phase lag leads particles to follow circular orbits and suppress the polar motion. In addition, this can adjust the direction of particle motion. There exists an optimal value of polar interaction strength at which the rectification is maximal. These results open the way for many application processes, such as spatial sorting of particles mixture and separation based on their physical properties.

Keywords: Brownian motion, self-propelled particles, stochastic processes

PACS: 05.40.–a, 45.50.–j, 02.50.–r **DOI:** 10.1088/1674-1056/ac3391

1. Introduction

Self-propelled particles can take energy from the environment and propel themselves into an out-of-equilibrium state.[1,2] Due to the sustained energy uptake and dissipation at the scale of the active unit, these systems exhibit several exotic phenomena that are inaccessible in systems at thermal equilibrium, for instance, swarming, flocking, and the emergence of other collective properties. The phenomenon of collective motion can be observed on vastly different length scales, including in schools of fish,[3] insect groups,[4,5] collections of gliding bacteria,[6–8] driven biopolymers,[9,10] and cellular flows in extended tissues.[11,12]

The external unbiased force can cause the directed motion of the diffusing particles in the ratchet system, which is called rectification. Generally speaking, the ratchet model with rectification can be divided into the following three types:[13] (i) Rocking ratchet:[14–16] the transient time asymmetry of the system is caused by the unbiased external force. (ii) Flashing ratchet:[17,18] the asymmetric potential field of the particle randomly transitions between two or more states or adopts the time modulation of the potential to form a directed motion. (iii) Correlation ratchet:[19,20] this model mainly considers the influence of color noise on rectification. In all of the above models, the unbiased driving force can break the thermodynamic equilibrium and induce the rectification of particles. Other types of ratchet models can be summarized as the above three types of extensions or their combinations. For example, a model based on a dual-noise, non-uniform temperature field and an asymmetric spatial environment can be attributed to a rocking ratchet. When the model is proposed in different states, or particles transition between multiple states, the system can be attributed to the flashing ratchet model. Researchers have committed to studying the rectification motion in asymmetric structures from various aspects, such as (i) particle classification: active particles,[21,22] polar particles,[23,24] chiral particles,[25] run-tumble particles,[26] and others. (ii) The physical properties of particles: size, shape, and mass.[27,28] (iii) Asymmetric structural properties: fixed structures[29] or structures with constant velocity.[30] Most studies on the transport of self-propelled particles have referred to the consideration of the overdamped regime. However, the overdamped approximation is not justified in many situations. The inertial effect of particles exhibits remarkable behaviors, including current reversals and chaotic transport.[31–33] In addition, different noise types[34–36] also have a great influence on the motion of underdamped particles.

Nikita and colleagues studied the stochastic dynamics of self-propelled particles with polar interaction subject to phase lag and revealed the existence of a traveling band, clouds, and vortical structures.[37] However, the influence of rectification has not been considered yet. In this paper, we extend this work[37] by studying the ratchet transport of underdamped particles with polar interaction subject to phase lag. We focus on finding how the inertia effect influences the rectification of particles and investigating the underlying mechanisms of polar interaction and phase lag.

†Corresponding author. E-mail: zhuweijing996@163.com

‡Corresponding author. E-mail: aibq@scnu.edu.cn

© 2022 Chinese Physical Society and IOP Publishing Ltd

2. Model and methods

We model N particles moving in a two-dimensional (2D) space with periodic boundary conditions along the x direction and hard wall boundary conditions along the y direction (see Fig. 1(a)). The shape of the spatially periodic channel is modeled by the half width $h(x)$,

$$h(x)=\begin{cases}\dfrac{W}{2}+\dfrac{H}{L_1}x, & 0\le x<L_1,\\ \dfrac{W}{2}+\dfrac{H}{L_2}(L-x), & L_1\le x<L,\end{cases} \tag{1}$$

where L corresponds to the periodic of the channel, and parameters W and $2H+W$ control the minimal and maximal channel width, respectively. The asymmetric parameter is denoted as $\Delta=(L_1-L_2)/L$. The reflecting channel boundaries are defined by Eq. (1), which ensures the confinement of particles inside the channel.[22] The coordinates of particles $i=1,\ldots,N$ can be described by $\boldsymbol{r}_i\equiv(x_i,y_i)$ and they are oriented at the angle θ_i of the polar axis $\boldsymbol{n}_i\equiv(\cos\theta_i,\sin\theta_i)$. We consider the short range interaction force, $\boldsymbol{F}_i=F_i^x\boldsymbol{e}_x+F_i^y\boldsymbol{e}_y=\sum\boldsymbol{F}_{ij}$, acting on particle–particle interactions. Particle i evolves according to the following Langevin equation:

$$m\frac{\mathrm{d}^2x_i}{\mathrm{d}t^2}=-\Gamma\frac{\mathrm{d}x_i}{\mathrm{d}t}+f_0\cos\theta_i+F_i^x, \tag{2}$$

$$m\frac{\mathrm{d}^2y_i}{\mathrm{d}t^2}=-\Gamma\frac{\mathrm{d}y_i}{\mathrm{d}t}+f_0\sin\theta_i+F_i^y, \tag{3}$$

$$\frac{\mathrm{d}\theta_i}{\mathrm{d}t}=\frac{g}{|Z_\rho^i|}\sum_{j\varepsilon Z_\rho^i}\sin(\theta_j-\theta_i-\alpha)+\sqrt{2D_\theta}\xi_{\theta_i}(t), \tag{4}$$

where m is the mass of the particles, Γ is the Stokes friction coefficient, f_0 is the self-propelled force and D_θ is the rotational diffusion coefficient. $\xi_{\theta_i}(t)$ denotes zero mean white noise with the relation $\langle\xi_{\theta_i}(t)\xi_{\theta_j}(t')\rangle=\delta_{\theta_i\theta_j}\delta(t-t')$.

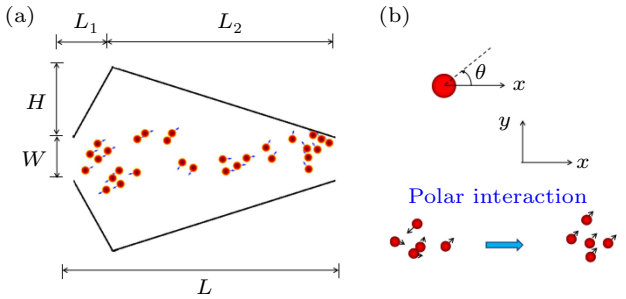


Fig. 1. (a) Schematic illustration of the ratchet device: self-propelled particles move in a two-dimensional periodic channel with periodicity L. The reflecting channel boundaries are defined by Eq. (1), which ensures the confinement of particles inside the channel. (b) Schematic diagram of the polar interaction case. Polar interaction leads to the parallel alignment of the velocity of moving objects.

According to Eq. (4), we consider the polar interaction of particles, and particles interact with each other within a radius ρ. Each particle adjusts its direction of motion to the average motion direction of the neighborhood Z_ρ^i. Z_ρ^i denotes the cardinality of the set of all neighbors. The set of all neighbors for a particle i obeys the following equation:

$$Z_\rho^i=\{j|j\in\{1,\ldots,N\}\backslash i,(x_i-x_j)^2+(y_i-y_j)^2\le\rho^2\}. \tag{5}$$

Polar interaction is controlled by a coupling strength g and additionally adds a phase lag parameter α. The orientational order can be characterized by the polar order parameter P,[38–40]

$$P=\left\langle\left|\frac{1}{N}\sum_{j=1}^{N}\mathrm{e}^{\mathrm{i}\theta_j(t)}\right|\right\rangle, \tag{6}$$

where $\langle\cdots\rangle$ denotes time average. Here, $P\to1$ represents particles moving in the same direction, $P\to0$ represents particles moving in any direction.

Pairs of particles i and j interact through a stiff repulsive harmonic force, $\boldsymbol{F}_{ij}=k(r_{ij}-2r)\hat{\boldsymbol{r}}_{ij}$ when $r_{ij}<2r$ ($\boldsymbol{F}_{ij}=0$ otherwise). r denotes the radius of the particle, k is the spring constant, and $r_{ij}=|\boldsymbol{r}_i-\boldsymbol{r}_j|$ and $\hat{\boldsymbol{r}}_{ij}=(\boldsymbol{r}_i-\boldsymbol{r}_j)/r_{ij}$. In order to mimic hard particles, we use a larger value for the product of the spring constant, thus ensuring that the particle overlaps decay quickly.

Before the statistical simulation, we can rewrite Eqs. (2)–(4) in the dimensionless forms, giving the characteristic length scale $\hat{x}=x/L$, $\hat{y}=y/L$ and the timescale $\hat{t}=t/\tau_0$, $\tau_0^2=mL$.

$$\frac{\mathrm{d}^2\hat{x}_i}{\mathrm{d}\hat{t}^2}=-\hat{\Gamma}\frac{\mathrm{d}\hat{x}_i}{\mathrm{d}\hat{t}}+\hat{f}_0\cos\hat{\theta}_i+\hat{F}_i^x, \tag{7}$$

$$\frac{\mathrm{d}^2\hat{y}_i}{\mathrm{d}\hat{t}^2}=-\hat{\Gamma}\frac{\mathrm{d}\hat{y}_i}{\mathrm{d}\hat{t}}+f_0\sin\hat{\theta}_i+\hat{F}_i^y, \tag{8}$$

$$\frac{\mathrm{d}\theta_i}{\mathrm{d}\hat{t}}=\hat{g}\sum_{j\varepsilon Z_\rho^i}\sin(\theta_j-\theta_i-\hat{\alpha})+\sqrt{2\hat{D}_\theta}\hat{\xi}_{\theta_i}(\hat{t}), \tag{9}$$

where $\hat{\Gamma}=(\tau_0/m)\Gamma$, $\hat{g}=(g/|Z_\rho^i|)\tau_0$, $\hat{\alpha}=\alpha\tau_0$, $\hat{D}_\theta=D_\theta\tau_0$, and $\hat{\chi}=(\chi/L)$ $(\chi=L_1,L_2,r,W,H)$. From now on, we will only use the dimensionless variables and omit the hat for all quantities appearing in the above equations.

In this paper, we use the second-order stochastic Runge–Kutta algorithm. To characterize the particles' drift in the absence of external biases, the average velocity along the x-direction can be obtained as $v_{\theta_0}=\lim_{t\to\infty}(\langle x(t)\rangle_{\theta_0}/t)$, where θ_0 is the initial angle of the trajectory. The rectification power after a second average over all θ_0 is

$$v=\frac{1}{2\pi}\int_0^{2\pi}\mathrm{d}\theta_0 v_{\theta_0}. \tag{10}$$

The area coverage of the self-propelled particles is $\phi_\mathrm{a}=N\pi r^2/L(H+W)$.

3. Results and discussion

In the simulation results, the initial position of the particles is randomly distributed in the sample; meanwhile, orientations are also random over the interval $[0,2\pi]$. We have chosen less than 10^{-3} integration step time and over 10^7 simulation

time to reach a steady state. Unless otherwise illustrated, the set parameters are $H = 4.0$, $L = 15.0$, $\Delta = -0.7$, $r = 0.5$, and $\phi_a = 0.2$.

Actually, there are two critical elements of the ratchet setup in nonlinear systems.[41] One is the asymmetry (temporal and/or spatial) that can violate the left–right symmetry of the response because transport in a fully symmetrical system is unbiased. The other is the fluctuating input zero-mean force: it should break the thermodynamical equilibrium, which prevents the appearance of any directed transport due to the second law of thermodynamics. For our system, the asymmetry comes from the left–right asymmetry of the channel and the fluctuating input zero-mean force comes from the self-propulsion of active particles.

Figure 2 describes the average velocity v as a function of the self-propelled force f_0 for various values α. When $f_0 \to 0$, particles can be seen as passive and the self-propulsion disappears; thus, the average velocity is not obvious. When $f_0 \to \infty$, no external ratchet mechanism is applied to the particles; this means that the symmetry of the system cannot be broken and thus v drops to zero. In order to discuss this in detail, we compare $-\Gamma \frac{dx}{dt} + f_0 \cos\theta(t)$ for the underdamped case (see Fig. 2(a)) and $f_0 \cos\theta(t)$ for the overdamped case (see Fig. 2(b)).

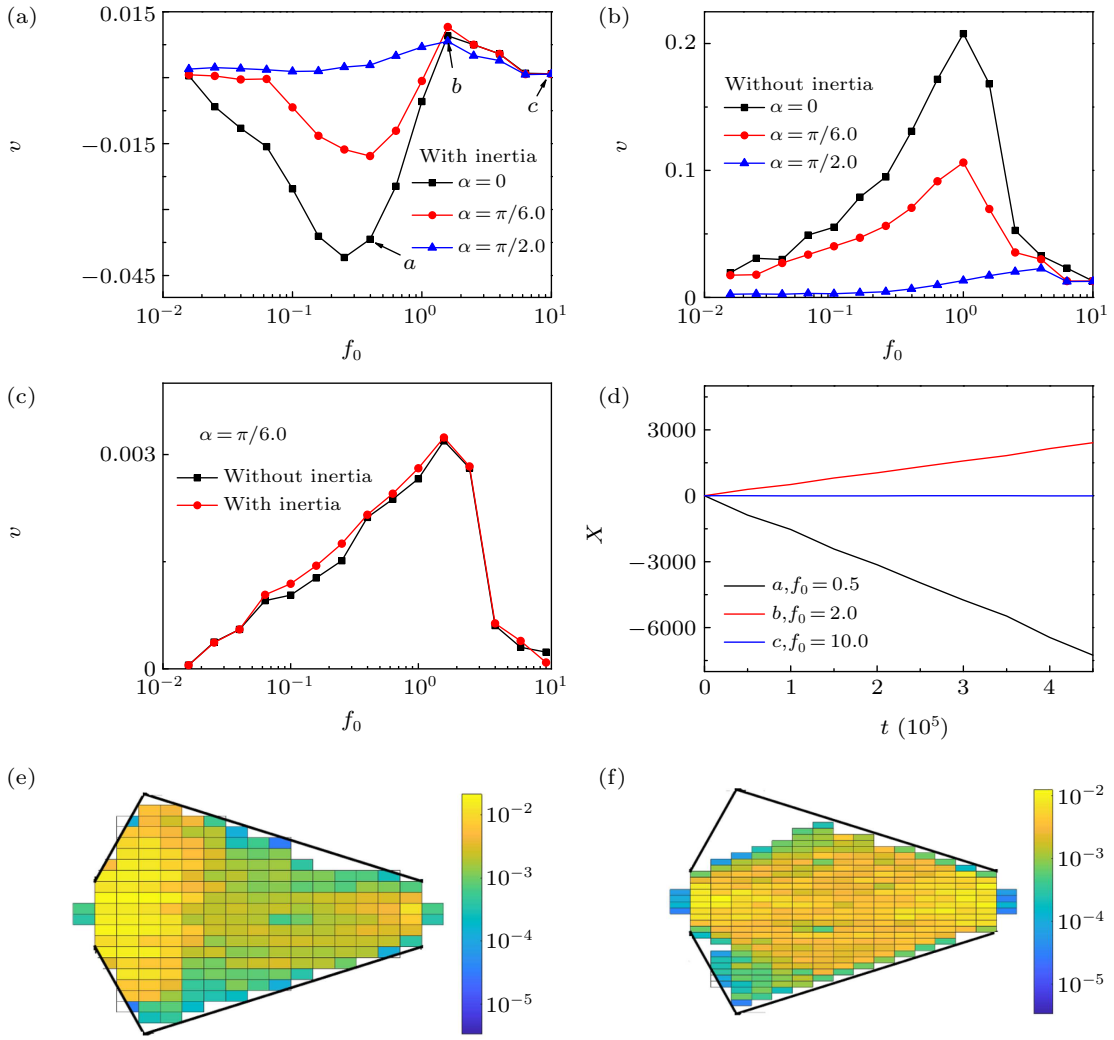


Fig. 2. Average velocity v *versus* the self-propelled force f_0 for various values α at $\Gamma = 3.0$. (a) Underdamped case (with the inertial term). (b) Overdamped case (without the inertial term). (c) Average velocity v *versus* the self-propelled force f_0 at $\Gamma = 30.0$ and $\alpha = \pi/6.0$ when the inertial term is included and neglected. (d) Description of the average position x *versus* time starting from the random initial condition for various values f_0, corresponding to a, b, c in Fig. 2(a). (e) 2D histogram of particle probability density distribution corresponding to a in Fig. 2(a). (f) 2D histogram of particle probability density distribution corresponding to b in Fig. 2(a). The other parameters are $D_\theta = 0.01$, $\rho = 1.5$, $W = 3.0$, and $g = 0.1$.

For the overdamped case (without inertial term) shown in Fig. 2(b), the particle always moves along the easy direction of the substrate asymmetry (positive v) and no current reversals occur. The ratchet phenomenon can be explained as follows. Note that Δ controls the direction of the average velocity. When $\Delta = -0.7$, the left side of the structure is steeper and it is easier for particles to move toward the slanted side than toward the steeper side, so on average particles move to the right (positive average velocity). It is important to note that in the overdamped limit current reversals of the non-active particles can be induced by several combined rectification mechanisms in complex systems.[42,43] However, in our simple system, the

ratchet effect only occurs in a single direction when the inertia is neglected.

For the underdamped case (with the inertial term) shown in Fig. 2(a), the transport behaviors become complex. For the certain value of α, upon increasing f_0, the average velocity firstly increases to its negative maximal value, then decreases, and finally reverses its direction. The most important feature for the underdamped case is the occurrence of current reversal. This phenomenon is also a common feature in collectively interacting non-active systems,[44–46] where the reversal mechanism is different from that in the present system.

Now we will explain the above behaviors. The direction of transport is determined by the competition between the slope of the structure and the distance from the lowest to the highest part of the asymmetric structure. When the distance from the lowest to the highest part of the asymmetric structure dominates the transport (particles can easily pass the barrier), and the distance from the slanted side is longer than the steep side, the particles are easily thrown out from the steep side, resulting in negative average velocity. As shown in Fig. 2(e), most of the particles are concentrated on the steep side; thus, on average the average velocity is negative. As f_0 increases, the effect of inertia weakens; the slope of the structure dominates the transport (particles cannot easily pass the barrier), and the left side of the asymmetric structure is steeper and thus particles prefer to gather on the slanted side (see Fig. 2(f)), resulting in particles on average moving to the right. Of course, if the structure is negligible, the ratchet effect will disappear. Note that the direction of the particles also depends on the magnitude of α; please refer to Fig. 5 for a specific explanation. For a very large value of Γ (*e.g.*, $\Gamma = 30.0$), shown in Fig. 2(c), the system reduces to its overdamped version and thus the curves are almost identical for both underdamped and overdamped cases.

In Fig. 2(d), we plot the average position x of particles as a function of the time t starting from the random initial condition for various values f_0, corresponding to a, b, c in Fig. 2(a). At a and b, $|x|$ increases over a long period of time, which means that particles continuously flow in the right (or left) direction near the optimal value f_0. At c, x is near zero for a long time, illustrating that the directed transport is destroyed for large f_0.

The dependence of the average velocity v on the friction coefficient Γ for various values α are presented in Fig. 3. In the underdamped regime, at short timescales ($t \ll 1/\Gamma$), the dynamic of particles is dominated by inertia and the trajectory cannot be self-similar, which is termed "ballistic Brownian motion".[47] In the overdamped regime, particles show diffusive motion at short timescales.[48] According to Eq. (7), there exists competition between the friction coefficient Γ and the self-propelled force f_0. This means that at small values of Γ, the self-propulsion force plays a key role in transport and thus the average velocity is prominent. When $\Gamma \to \infty$, the self-propulsion force is completely suppressed and rectification is destroyed, thus $v \to 0$. However, for intermediate values of Γ (*e.g.* $1.0 < \Gamma < 10.0$) and desirable values of f_0 (*e.g.* $f_0 = 0.5$ see Fig. 3(a)), the distance from the lowest to the highest part of the asymmetric structure dominates the transport; the particles are easily thrown out from the steep side and thus the average velocity is negative. However, for the case of $f_0 = 2.0$ [see Fig. 3(b)], the slope of the structure dominates the transport; the average velocity is always positive and there exists an optimal value of Γ at which v is maximal.

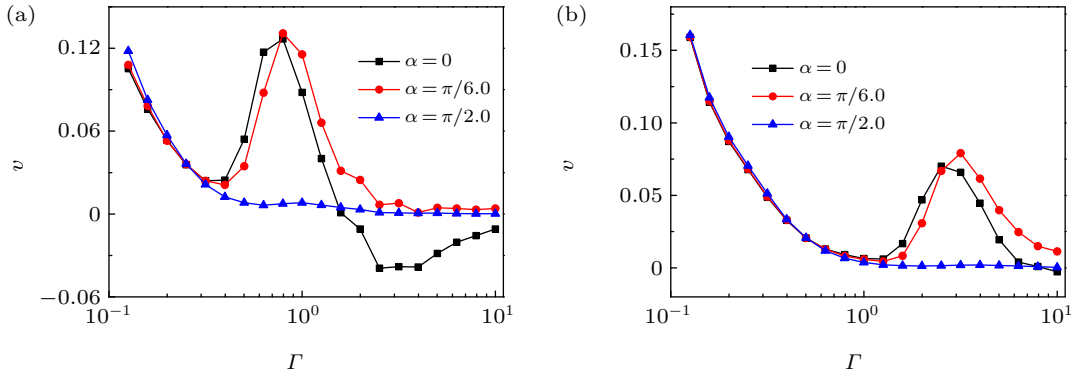


Fig. 3. Average velocity v *versus* the friction coefficient Γ for various values α. (a) Self-propelled force $f_0 = 0.5$. (b) Self-propelled force $f_0 = 2.0$. The other parameters are $D_\theta = 0.01$, $W = 3.0$, $\rho = 1.5$, and $g = 0.1$.

We present the average velocity v *versus* the polar interaction strength g for various α in Fig. 4. When the polar interaction is considered, particles show clustering behaviors. Note that the size of the cluster increases with polar interaction strength. When $g \to 0$, the polar interaction can be ignored and particles cannot form a cluster. As g increases, the polar interaction takes effect and particles form some clusters. Also, the clusters begin to interact with asymmetric structures. For the case of $f_0 = 0.5$, shown in Fig. 4(a), particles are very sensitive to the distance from the lowest to the highest part of the asymmetric structure and particles can be easily thrown out from the steep (left) side, resulting in negative average velocity. For the case of $f_0 = 2.0$,

shown in Fig. 4(b), the slope of the structure dominates the transport and thus the average velocity is always positive. When $g \to \infty$, all particles form a big cluster and the effect of asymmetric structures is negligible; the ratchet effect will disappear and thus v reduces to zero. The corresponding polar order parameter P as a function of g is plotted in Fig. 4(c). Because the polar interaction dominates the transport, particles move in the same direction and form a big cluster (see Fig. 4(d)), leading $P \to 1$.

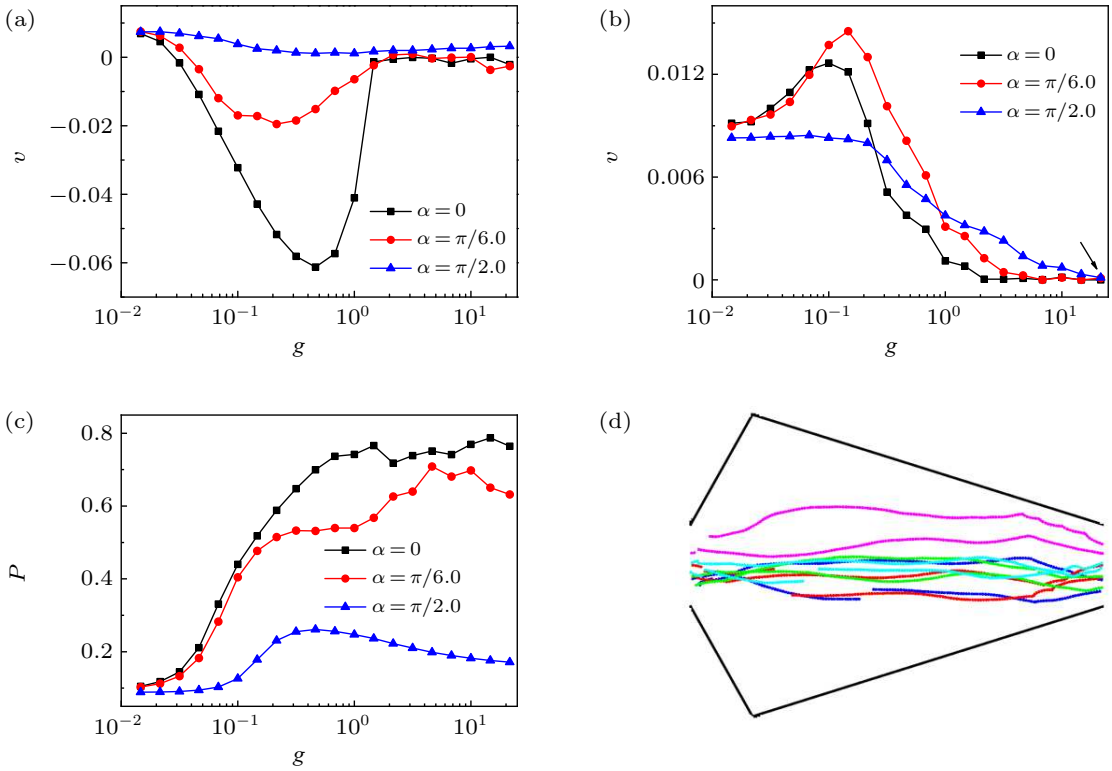


Fig. 4. Average velocity v *versus* the polar interaction strength g for various values α at $\Gamma = 3.0$. (a) Self-propelled force $f_0 = 0.5$. (b) Self-propelled force $f_0 = 2.0$. (c) Polar order parameter P as a function of the polar interaction strength g for various values α at $\Gamma = 3.0$ and $f_0 = 2.0$. (d) Representative trajectories of particles (different particles are differentiated by color) moving inside the channel at $g = 21$ and $\alpha = 0.0$ described by a in panel (b). The other parameters are $D_\theta = 0.01$, $W = 3.0$, and $\rho = 1.5$.

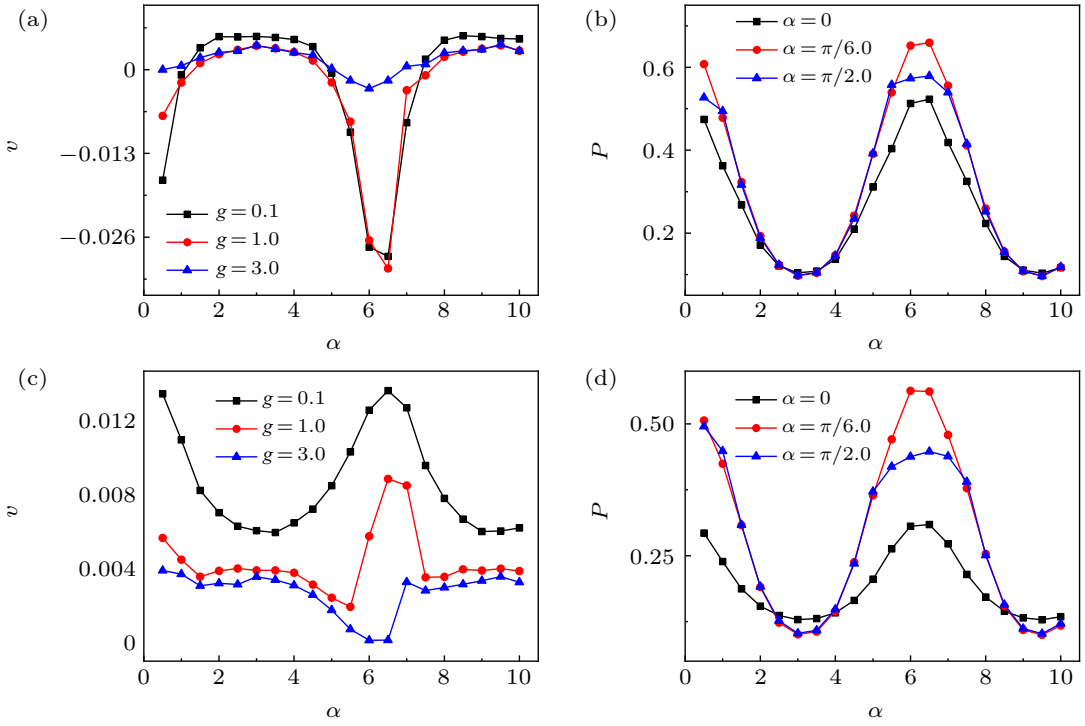


Fig. 5. Average velocity v and polar order parameter P *versus* the phase lag α for various values g at $\Gamma = 3.0$. (a) and (b) The self-propelled force $f_0 = 0.5$. (c) and (d) The self-propelled force $f_0 = 2.0$. The other parameters are $D_\theta = 0.01$, $W = 3.0$, and $\rho = 1.5$.

Figures 5(a) and 5(b) show the average velocity v and polar order parameter P over the phase lag α. For $\alpha = 0$, we can feature the phenomenology of the Vicsek model. In this model, two solutions are possible: one observes the formation of the polar order when the noise is small, whereas particles exhibit disordered motion. Due to the current value of the rotational diffusion coefficient $D_\theta = 0.01$, our system satisfies the former scenario. In this case ($\alpha = 0.0$), particles form some clusters and P attains a maximal value, shown in Figs. 5(b) and 5(d). The presence of the phase lag causes the synchronized particle system to start rotating (see the trajectory of the particles in Fig. 6(a)), which suppresses the rectification and polar strength. Therefore, both the average velocity and the polar order decrease. The introduction of phase lag can be considered as a substitution of chirality explicitly by the rotation frequency of each particle.[37,49,50] In addition, when we perform analysis of the right-hand side of Eq. (9), it is found that the term of α has a periodic effect on the rectification. Thus, the above discussion is valid only based on the minimum period regime of α.

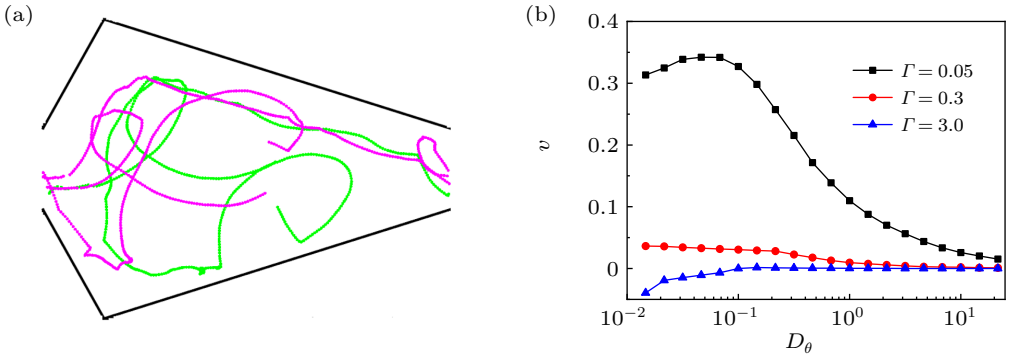


Fig. 6. (a) Representative trajectories of particles (different particles are differentiated by color) illustrate the underlying mechanics between α and the polar interaction: for large α ($\alpha = \pi/2.0$), particles follow circular orbits and frustrate the polar interaction. The other parameters are $g = 1.0$, $D_\theta = 0.01$, $\rho = 1.5$, $W = 3.0$, and $f_0 = 2.0$. (b) Dependence of the average velocity v on the rotational diffusion coefficient D_θ for various values Γ. The other parameters are $f_0 = 0.5$, $g = 0.1$, $\alpha = 0.0$, $W = 3.0$, and $\rho = 1.5$.

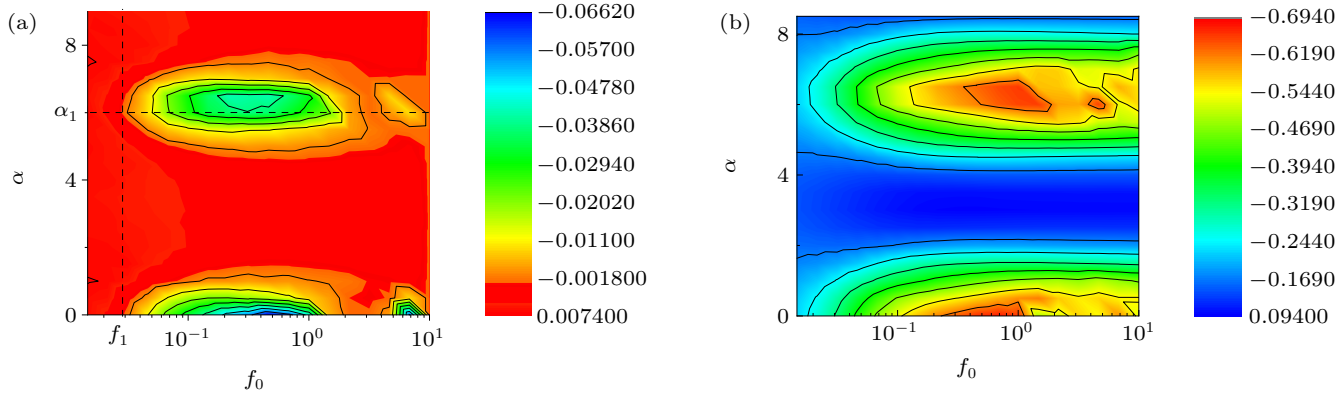


Fig. 7. (a) Contour plots of v as a function of f_0 and α. (b) Contour plots of P as a function of f_0 and α. The other parameters are $D_\theta = 0.01$, $g = 0.1$, $\Gamma = 3.0$, $W = 3.0$, and $\rho = 1.5$.

Figure 6(b) depicts the impact of the rotational diffusion coefficient D_θ on the rectification of self-propelled particles. The correlation function of the orientation is expressed as $\langle \boldsymbol{n}(t) \cdot \boldsymbol{n}(t') \rangle = \mathrm{e}^{-D_\theta |t - t'|}$.[51] When $D_\theta \to \infty$, this correlation converts to the delta function, the persistence length decreases (eventually vanishes) and the self-propelled force acts as a zero mean white noise; thus, the system is in equilibrium and the rectification disappears. When D_θ is small, the curves $v(D_\theta)$ are different for two cases: (A) for the damping case (*e.g.* $\Gamma = 0.3, 3.0$) and (B) for the weak damping case (*e.g.* $\Gamma = 0.05$). For the damping case ($\Gamma = 0.3, 3.0$), the momentum relaxation time $\tau = 1/\Gamma$ is far less than the persistence time $\tau_\mathrm{p} = 1/D_\theta = 100$. Thus, rotational diffusion dominates the transport; this case is similar to the adiabatic regime in the forced thermal ratchet.[52] This means that the self-propelled angle θ_i remains nearly the same and the average velocity approaches its maximal values. For the weak damping case (*e.g.* $\Gamma = 0.05$), the momentum relaxation time τ becomes large, and the damping process competes with the rotational diffusion. When increasing D_θ from zero, the thermal noise, by pulling the particles towards the channel, acts as lubricant and thus the average velocity increases. When $D_\theta \to \infty$, the system begins Brownian motion and becomes homogeneous, thus suppressing the rectification.

To investigate the dependence of v and P on α and f_0 in detail, we show the contour plots v and P as a function of α and f_0 in Figs. 7(a) and 7(b). By adjusting f_0 and α, the curves of v and P change periodically. When α is increased

from zero, the average velocity is always positive at $f_0 < f_1$; interestingly, in the period range of $\alpha \in [0, 2\pi]$ $(0 < \alpha < \alpha_1)$, the particle changes its direction twice at $f_0 > f_1$. The critical values of f_1 and α_1 depend on the system parameters.

4. Conclusion

In this work, we have numerically studied the ratchet transport of underdamped particles subject to phase lag in a 2D asymmetric channel. We found that when the inertial term is included, the transport behaviors become complex. For very small values of Γ, the average velocity is always positive. For intermediate values of Γ, the average velocity is negative for a small self-propelled force and positive for a large self-propelled force. For very large values of Γ, the system can be reduced to an overdamped version. In addition, there exists an optimal value of the polar interaction strength at which the rectification is maximal. We have shown that it is possible to change the direction of the particles in the presence of α. On increasing the phase lag from zero, the average velocity can change its direction serval times for characteristics of critical f_0. Moreover, by introducing the phase lag, particles start to rotate and might suppress the rectification. For the damping case, the average velocity decreases monotonously with increasing D_θ; however, for the weak damping case, there exists an optimal value of D_θ at which the average velocity is maximal.

Acknowledgments

Project supported by the National Natural Science Foundation of China (Grant No. 12075090), the Key-Area Research and Development Program of Guangdong Province, China (Grant No. 2019B030330001), the Science and Technology Program of Guangzhou City (Grant No. 2019050001), the Natural Science Foundation of Guangdong Province, China (Grant No. 2017A030313029), and the Major Basic Research Project of Guangdong Province, China (Grant No. 2017KZDXM024).

References

[1] Ramaswamy S 2010 *Annu. Rev. Condens. Matter Phys.* **1** 323
[2] Erdmann U, Ebeling W, Schimansky-Geier L and Schweitzer F 2000 *Eur. Phys. J. B* **15** 105
[3] Lopez U, Gautrais J, Couzin I D and Theraulaz G 2012 *Interface Focus* **2** 693
[4] Buhl J, Sumpter D J T, Couzin I D, Hale J J, Despland E, Miller E R and Simpson S J 2006 *Science* **312** 1402
[5] Bazazi S, Buhl J, Hale J J, Anstey M L, Sword G A, Simpson S J and Couzin I D 2008 *Curr. Biol.* **18** 735
[6] Dombrowski C, Cisneros L, Chatkaew S, Goldstein R E and Kessler J O 2004 *Phys. Rev. Lett.* **93** 098103
[7] Sokolov A, Aranson I S, Kessler J O and Goldstein R E 2007 *Phys. Rev. Lett.* **98** 158102
[8] Peruani F, StarrußJ, Jakovljevic V, Søgaard-Andersen L, Deutsch A and Bär M 2012 *Phys. Rev. Lett.* **108** 098102
[9] Schaller V, Weber C, Semmrich C, Frey E and Bausch A R 2010 *Nature* **467** 73
[10] Sumino Y, Nagai K H, Shitaka Y, Tanaka D, Yoshikawa K, Chaté H and Oiwa K 2012 *Nature* **483** 448
[11] Trepat X, Wasserman M R, Angelini T E, Millet E, Weitz D A, Butler J P and Fredberg J J 2009 *Nat. Phys.* **5** 426
[12] Serra-Picamal X, Conte V, Vincent R, Anon E, Tambe D T, Bazellieres E, Butler J P, Fredberg J J and Trepat X 2012 *Nat. Phys.* **8** 628
[13] DeSilva A W and Katsouros J D 1999 *Phys. Rev. E* **59** 3774
[14] Schreier M, Reimann P, Hänggi P and Pollak E 1998 *Europhys. Lett.* **44** 416
[15] Mateos J L 2000 *Phys. Rev. Lett.* **84** 258
[16] Borromeo M, Costantini G and Marchesoni F 2002 *Phys. Rev. E* **65** 041110
[17] Astumian R D and Bier M 1994 *Phys. Rev. Lett.* **72** 1766
[18] Rousselet J, Salome L, Ajdari A and Prostt J 1994 *Nature* **370** 446
[19] Mei D, Xie C and Zhang L 2003 *Phys. Rev. E* **68** 051102
[20] Wolgemuth C, Hoiczyk E, Kaiser D and Oster G 2002 *Curr. Biol.* **12** 369
[21] Wan M B, Reichhardt C J O, Nussinov Z and Reichhardt C 2008 *Phys. Rev. Lett.* **101** 018102
[22] Ghosh P K, Misko V R, Marchesoni F and Nori F 2013 *Phys. Rev. Lett.* **110** 268301
[23] Zhu W J, Li F G and Ai B Q 2017 *Eur. Phys. J. E* **40** 59
[24] Zhu W J, Huang X Q and Ai B Q 2009 *Physica A* **551** 124548
[25] Nourhani A, Crespi V H and Lammert P E 2015 *Phys. Rev. Lett.* **115** 118101
[26] Angelani L, Leonardo R D and Ruocco G 2009 *Phys. Rev. Lett.* **102** 048104
[27] Hänggi P and Marchesoni F 2009 *Rev. Mod. Phys.* **81** 387
[28] Hänggi P, Marchesoni F and Nori F 2005 *Ann. Phys.* **14** 51
[29] Kaiser A, Wensink H H and Löwen H 2012 *Phys. Rev. Lett.* **108** 268307
[30] Kaiser A, Popowa K, Wensink H H and Löwen H 2013 *Phys. Rev. E* **88** 022311
[31] Nagai K H, Sumino Y, Montagne R, Aranson I S and Chaté H 2015 *Phys. Rev. Lett.* **114** 168001
[32] Sharma R and Velev O D 2015 *Adv. Funct. Mater.* **25** 5512
[33] Ivlev A V, Bartnick J, Heinen M, Du C R, Nosenko V and Löwen H 2015 *Phys. Rev. X* **5** 011035
[34] Liu R N and Kang Y M 2018 *Phys. Lett. A* **382** 1656
[35] Kostur M, Łuczka J and Hänggi P 2009 *Phys. Rev. E* **80** 051121
[36] Wu J C, An M and Ma W G 2019 *Soft Matter* **15** 7187
[37] Kruk N, Carrillo J A and Koeppl H 2020 *Phys. Rev. E* **102** 022604
[38] Ginelli F, Peruani F, Bär M, Chaté H 2010 *Phys. Rev. Lett.* **104** 184502
[39] Ngo S, Ginelli F, Chaté H 2012 *Phys. Rev. E* **86** 050101
[40] Peruani F, Ginelli F, Bär M, Chaté H 2011 *J. Phys.: Conf. Ser.* **297** 012014
[41] Denisov S, Hänggi P and Mateos J L 2009 *Am. J. Phys.* **77** 602
[42] Malgaretti P, Pagonabarraga I and Rubi J M 2013 *J. Chem. Phys.* **138** 194906
[43] Reimann P 2002 *Phys. Rep.* **361** 57
[44] de Souza Silva C C, Van de Vondel J, Morelle M and Moshchalkov V V 2006 *Nature* **440** 651
[45] Reichhardt C, Ray D and Olson Reichhardt C J 2015 *Phys. Rev. B* **91** 184502
[46] Perez de Lara D, Erekhinsky M, Gonzalez E M, Rosen Y J, Schuller I K and Vicent J L 2011 *Phys. Rev. B* **83** 174507
[47] Li T and Raizen M G 2013 *Ann. Phys.* **525** 281
[48] Zheng X, Hagen B T, Kaiser A, Wu M, Cui H, Li Z S and Löwen H 2013 *Phys. Rev. E* **88** 032304
[49] Degond P, Dimarco G and Mac T B N 2014 *Math. Models Methods Appl. Sci.* **24** 277
[50] Liebchen B and Levis D 2017 *Phys. Rev. Lett.* **119** 058002
[51] Schienbein M and Gruler H 1993 *B. Math. Biol.* **55** 585
[52] Magnasco M O 1993 *Phys. Rev. Lett.* **71** 1477